Ann. Acad. Rom. Sci.
Ser. Math. Appl.
ISSN 2066-6594 Vol. 16, No. 2/2024

ON HIGHER ORDER DYNAMIC MODE DECOMPOSITION*

Gyurhan Nedzhibov†

Abstract

This paper introduces an alternative variant of Higher Order Dynamic Mode Decomposition (HODMD), which improves the standard approach from a computational point of view. In the new scheme, time-delayed snapshots are used along with the special form of the Koopman operator. An algorithm is derived that allows the calculation of novel decomposition in a stable and efficient way. This method is suitable in cases where standard Dynamic Mode Decomposition (DMD) is not applicable. These are dynamics that show limited spatial complexity, and a very large number of included frequencies. We illustrate and explain the new method using some classical and sample dynamics.

Keywords: Dynamic Mode Decomposition, DMD, delay embedding, Higher Order DMD, HODMD, Frobenius companion matrix.

MSC: 65P02, 37M02.

DOI https://doi.org/10.56082/annalsarscimath.2024.2.265

1 Introduction

Dynamic Mode Decomposition (DMD) is an equation-free technique suitable for analyzing flow structures in numerical and experimental data, which has become very popular since it was first introduced in a paper by Schmid [1].

*Accepted for publication on June 15, 2024

†g.nedzhibov@shu.bg Faculty of Mathematics and Informatics, Shumen University, Shumen 9700, Bulgaria; paper written with financial support of Shumen University under Grant RD-21-342/01.03.2024

It has emerged as a leading technique to identify spatio-temporal coherent structures from high-dimensional data. Shortly after its introduction, it was shown by Rowley et al. [2] a close relation between the DMD and spectral analysis of the Koopman operator, see also [3]. DMD analysis can be considered as a numerical approximation to Koopman spectral analysis, and in this sense it is applicable to nonlinear dynamical systems.

Due to the widespread success of DMD, mainly based on its possibility of being applied easily to analyze many types of data, several researchers have focused their effort on varying the algorithm with the aim of increasing its robustness and its range of applications [4, 5, 6]. More examples are presented in detail in the review article by Rowley and Dawson [7], see also a recent review paper by Schmid [8]. See for theoretical work on the relationships of the DMD method with other methods, such as POD [9], Fourier analysis [4] and Koopman spectral analysis [2, 10, 11]. Theorems regarding the existence and uniqueness of DMD modes and eigenvalues can be found in [4]. For a review of the DMD literature, we refer the reader to [12, 13, 14].

In the present article, the so-called *Higher Order DMD* (HODMD) will play a central role. HODMD is an algorithm recently introduced by Clainche and Vega in [15] as an extension of classical DMD. As in the classical DMD approach, HODMD gives an approximation of the Koopman modes and calculates spatio-temporal structures as an expansion in terms of DMD modes and their associated frequencies, growth rates, and amplitudes. This extension uses delayed snapshots, which is a well known feature to increase observability. HODMD widens the range of applicability of DMD to cases in which the number of spatial modes is smaller than the number of frequencies describing the flow field. This scenario is mainly found in three types of applications: when the number of spatial points in the domain analyzed is restricted, when the data are too noisy and in transient dynamics. The main success of HODMD lies in its capability of analyzing highly complex (periodic and quasi-periodic) spatio-temporal data as an expansion of DMD modes that oscillate with a single temporal frequency for each one.

The HODMD framework has many advantages over the standard DMD approach. Among the most important advantages are:

Better at capturing non-linear dynamics: Traditional DMD is inherently a linear method, which may not effectively capture the dynamics of nonlinear systems. HODMD extends the method by incorporating higher-order interactions, making it more capable of representing and analyzing nonlinear dynamics.

Improved Accuracy: By considering higher-order terms, HODMD can

provide a more accurate representation of dynamics. This results in better reconstruction and prediction of the system's behavior, especially for systems with significant nonlinear interactions.

Scalability: HODMD can be applied to large datasets and complex systems, making it suitable for a wide range of applications, including fluid dynamics, neuroscience, structural health monitoring, and more. Its scalability allows it to handle high-dimensional data effectively.

Flexible Framework: The HODMD framework can be adapted to various types of data and systems. It can be applied to both time-series data and spatial-temporal data, providing flexibility in its application across different fields and types of problems.

The standard HODM framework does not explicitly exploit the special structure of the Koopman operator as a block companion (Frobenius) matrix. Our goal in this paper is to present an alternative algorithm for the HODMD method that utilizes the time-delayed snapshot approach and exploits the special form of the Koopman operator. The new scheme will preserve the above-described advantages of the HODMD approach over the standard DMD method. It will have the following advantages over the standard HODMD scheme:

Compactness: The block companion matrix form of the Koopman operator provides a more compact representation of the reduced DMD operator. This can reduce the dimensionality of the problem and the computational resources required.

Reduced Complexity: The new approach gives identical results to the standard HODMD approach, but with less computational complexity.

Faster Computation: By using a simpler structure for the reduced DMD operator the computational cost in the novel scheme is reduced, resulting in faster computations and more scalable algorithms.

Memory and Storage Efficiency: The compact representation of the reduced DMD operator leads to significant memory savings, which reduce overall data storage requirements, leading to more efficient data management.

The remainder of this work is organized as follows: in the rest of Section 1, for completeness of the exposition, we describe the standard DMD approach, HODMD and Delay coordinate based DMD, in Section 2, we propose and discuss a new approach for HODMD computation and in Section 3 we present examples demonstrating the new algorithm. The conclusion is in Section 4.

1.1 Standard DMD method

In this paragraph the DMD algorithm is briefly reviewed. The standard definition of DMD considers a sequential set of data

$$\mathcal{D} = \{\mathbf{z}_0, \ldots, \mathbf{z}_m\}, \tag{1}$$

where each $\mathbf{z}_k \in \mathbf{R}^n$, and $\mathbf{z}_i$ being a snapshot of the system state. The data could be from measurements, experiments or simulations collected at time t_i from a given nonlinear system. Assume that the data are equispaced in time, with a time step $\triangle t$ and the collection time starts from t_0 to t_m. The main assumption of the method is that there exists a linear (unknown) matrix A relating $\mathbf{z}_k$ to the subsequent $\mathbf{z}_{k+1}$:

$$\mathbf{z}_{k+1} = A\mathbf{z}_k \tag{2}$$

for $k = 0, \ldots, m-1$. The eigenvalues of A contain information on the growth or decay rates and frequencies of oscillations, which when combined represent the time evolution of the dynamical system. The DMD modes and eigenvalues are intended to approximate the eigenvectors and eigenvalues of A. The DMD method uses the arrangement of the data set into two large data matrices:

$$X = [\mathbf{z}_0, \ldots, \mathbf{z}_{m-1}] \quad \text{and} \quad Y = [\mathbf{z}_1, \ldots, \mathbf{z}_m], \tag{3}$$

such that $AX = Y$ and therefore $A = YX^\dagger$, where $X^\dagger$ is a Moore-Penrose pseudoinverse of X. In practice, the matrix A can be very high dimensional, so it is approximated by a lower order matrix to determine its leading spectral decomposition. Usually, the projection matrix of A onto the subspace spanned by the snapshots in X is performed. From the reduced singular value decomposition (SVD) of X

$$X = U\Sigma V^*,$$

where U, V are unitary matrices and Σ is a diagonal matrix, we can deduce the projected operator

$$\tilde{A} = U^*AU = U^*YV\Sigma^{-1}, \tag{4}$$

such that its eigenvalues are also the eigenvalues of A. Therefore, from the spectral decomposition of $\tilde{A}$

$$\tilde{A}W = W\Lambda, \tag{5}$$

where $\Lambda = \text{diag}\{\lambda_j\}_{j=1}^r$ is the matrix of eigenvalues and W is the matrix of eigenvectors of $\tilde{A}$, we determine the leading decomposition of A. The DMD modes are computed by the formula

$$\Phi = YV\Sigma^{-1}W. \tag{6}$$

The modes in (6) are often called *exact DMD modes*, because Tu et al. [12] prove that these are exact eigenvectors of matrix A.

As a result we can reconstruct the approximate dynamics of the data set $\mathcal{D}$. The representation of data, at sampling instants $t_k = k\triangle t$, in terms of DMD is given by the linear model:

$$\mathbf{z}_{DMD}(k) = \Phi\Lambda^k\mathbf{b}, \tag{7}$$

where $\mathbf{b} = \Phi^\dagger\mathbf{z}_0$, and $\Phi^\dagger$ is the pseudo-inverse of Φ.

For convenience the DMD eigenvalues λ_j can be converted to Fourier modes as

$$\omega_j = \ln(\lambda_j)/\triangle t, \tag{8}$$

for $j = 1, \ldots, r$. Therefore the approximate solution at all times is given by

$$\mathbf{z}_{DMD}(t) = \Phi\exp(\Omega t)\mathbf{b}, \tag{9}$$

where the columns of Φ are the DMD modes, and $\Omega = \text{diag}\{\omega_j\}_{j=1}^r$ is a diagonal matrix with the entries corresponding eigenvalues ω_j. The vector $\mathbf{b}$ determines the weighting of each of the r modes, so that $\mathbf{z}_0 = \Phi\mathbf{b}$. Then the vector $\mathbf{z}_{DMD}(t)$ defines the state of the system at time t.

1.2 Delay embedding DMD method

Delay embedding is also an important technique when the temporal or spectral complexity of a dynamical system exceeds the spatial complexity, for example, in systems characterized by a broadband spectrum or spatially undersampled. In this case, we arrive at a "short-and-wide", rather than a "tall-and-skinny", data matrix $\mathcal{D}$, and the standard algorithm fails at extracting all relevant spectral features. In particular, a central problem with DMD that was first observed by Tu et al. [12], is that the standard DMD algorithm is unable to accurately represent a standing wave in the data. In these cases, the data often contain hidden temporal structures and underlying dynamics that are not readily apparent. This requires advanced analytical techniques to get meaningful conclusions from such data. One

such technique is *Delay Embedding* DMD (or *Hankel* DMD), which provides a comprehensive framework for analyzing and interpreting complex temporal dynamics.

Delay Embedding DMD overcomes several shortcomings of the standard DMD method by extending its capabilities to handle nonlinear dynamics, non-uniformly sampled data, long-term temporal behavior, high-dimensional datasets, and noisy data. This makes it a more versatile and robust technique for dynamic mode decomposition in various applications. The Taken's embedding theorem [19] provides a rigorous framework for analyzing the information content of measurements of a nonlinear dynamical system.

To implement delay embedding DMD, given the data sequence $\mathcal{D}$ in (1), we stack $s \leq m$ time-shifted copies of the data to form the augmented input matrix. The following Hankel matrix is formed:

$$\mathcal{D}_{aug} = \begin{bmatrix} \mathbf{z}_1 & \mathbf{z}_2 & \dots & \mathbf{z}_{m-s+1} \\ \mathbf{z}_2 & \mathbf{z}_3 & \dots & \mathbf{z}_{m-s+2} \\ \vdots & \vdots & \ddots & \vdots \\ \mathbf{z}_s & \mathbf{z}_{s+1} & \dots & \mathbf{z}_m \end{bmatrix}, \tag{10}$$

where the applied embedding dimension is s. The augmented data matrix $\mathcal{D}_{aug}$ is then used instead of $\mathcal{D}$ and processed by the standard DMD algorithm. The DMD algorithm prescribed in the previous section is applied to the augmented matrices $X_{aug}, Y_{aug} \in \mathbf{R}^{(n.s)\times(m-s)}$ instead of X and Y, giving eigenvalues Φ_{aug} and modes Λ_{aug}. The first n rows of Φ_{aug} correspond to the current (not shifted) time and are used to forecast $\mathbf{x}(t)$.

Among the reasons to compute DMD on these delay coordinates, in addition to the standing wave issue mentioned, is that if the state measurements are low dimensional, it may be necessary to increase the rank of the matrix X_{aug} by using delay coordinates. In general, we may increase the number s of delay coordinates until the system reaches full rank numerically, i.e., adding more rows only results in new singular values.

Arbabi and Mezić [16] have shown the convergence of this time-shifted approach to the eigenfunctions of the Koopman operator. They also illustrated remarkable improvements in the prediction of simple and complex fluid systems. Further examples and theoretical results on delay embedding and the Hankel viewpoint of Koopman analysis are given by Brunton et al. [17], Kamb et al. [18]. They have demonstrated that linear time-delayed models are an effective and efficient tool to capture nonlinear and chaotic dynamics.

1.3 Higher Order DMD method

The idea of an extension of the standard DMD from higher order that is capable of providing highly accurate results in cases in which the performance of the classical DMD is deteriorating or even fails. The objective is to mix the classical DMD with Taken's delay embedding theorem [19], leading to a higher order Koopman assumption that uses time-lagged snapshots, as

$$\mathbf{z}_{k+s} = A_1\mathbf{z}_k + A_2\mathbf{z}_{k+1} \ldots + A_s\mathbf{z}_{k+s-1}, \tag{11}$$

for $k = 1, \ldots, m-s$.

Let us note that $s \geq 1$ is adjustable and, when $s = 1$ this assumption exactly matches the standard Koopman assumption presented in Eq (2). The resulting mapping is given by

$$\mathcal{A}X_{aug} = Y_{aug}, \tag{12}$$

where X_{aug} and Y_{aug} are the augmented (Hankelized) data matrices:

$$X_{aug} = \begin{bmatrix} \mathbf{z}_1 & \ldots & \mathbf{z}_{m-s} \\ \mathbf{z}_2 & \ldots & \mathbf{z}_{m-s+1} \\ \vdots & \ldots & \vdots \\ \mathbf{z}_s & \ldots & \mathbf{z}_{m-1} \end{bmatrix} \text{ and } Y_{aug} = \begin{bmatrix} \mathbf{z}_2 & \ldots & \mathbf{z}_{m-s+1} \\ \mathbf{z}_3 & \ldots & \mathbf{z}_{m-s+2} \\ \vdots & \ldots & \vdots \\ \mathbf{z}_{s+1} & \ldots & \mathbf{z}_m \end{bmatrix} \tag{13}$$

and $\mathcal{A}$ is a block companion matrix:

$$\mathcal{A} = \begin{bmatrix} \mathbf{0} & \mathbf{I} & \mathbf{0} & \ldots & \mathbf{0} \\ \mathbf{0} & \mathbf{0} & \mathbf{I} & \ldots & \mathbf{0} \\ \vdots & \vdots & \ddots & \ddots & \vdots \\ \mathbf{0} & \mathbf{0} & \mathbf{0} & \ddots & \mathbf{I} \\ A_1 & A_2 & A_3 & \ldots & A_s \end{bmatrix}, \tag{14}$$

with $A_i \in \mathbf{R}^{n\times n}$, $\mathbf{0}$ is the $n \times n$ zero matrix and $\mathbf{I}$ is the $n \times n$ unit matrix. Using the augmented data matrices X_{aug} and Y_{aug} and the higher order Koopman operator $\mathcal{A}$, we can apply the core algorithm and extract spectral information from temporally broadband or spatially sparse data sequences. The higher-order extension adds more robustness and flexibility to the standard algorithm and enables the analysis of systems for which temporal resolution is substituted for spatial resolution.

Higher Order DMD was introduced by Le Clainche and Vega in [15]. However, the algorithm presented there does not exploit the special form of the generalized Koopman matrix $\mathcal{A}$ in (14). The proposed algorithm consists of the following two main steps:

1. Singular value decomposition (SVD) is applied to the full snapshot matrix $\mathcal{D}$ in (1):
$$\mathcal{D} = U_{\mathcal{D}} \Sigma_{\mathcal{D}} V_{\mathcal{D}}^*. \tag{15}$$

2. The delay-embedding DMD approach is applied to the reduced snapshot matrix
$$\hat{\mathcal{D}} = U_{\mathcal{D}}^* \mathcal{D}. \tag{16}$$

Therefore, the reduced order approximation of $\mathcal{A}$ is computed by the formula

$$\tilde{\mathcal{A}} = U_X^* \mathcal{A} U_X = U_X^* Y_{aug} V_X \Sigma_X^{-1}, \tag{17}$$

which corresponds to formula (4) in the one-dimensional case, where U_X is from the SVD of $X_{aug} = U_X \Sigma_X V_X^*$.

This means that the approach proposed in [15] is more of a Delay embedding DMD (or Hankel DMD) applied to the reduced data set

$$\hat{\mathcal{D}} = \{\hat{\mathbf{z}}_0, \ldots, \hat{\mathbf{z}}_m\}, \tag{18}$$

where $\mathbf{z}_i = U_{\mathcal{D}} \hat{\mathbf{z}}_i$ for $i = 0, \ldots, m$. We should note that in the algorithm presented in [15] the DMD amplitudes are calculated in a more optimal way than in the standard DMD approach.

2 A new approach to Higher Order DMD

Our goal in this section is to obtain an alternative approach to calculating the HODMD described in Section 1.3, which would be more cost effective. For this purpose, we will use the special form of the Koopman operator $\mathcal{A}$ defined in (14).

DMD operator as a block companion matrix

Let us represent operator $\mathcal{A} \in \mathbf{R}^{s.n \times s.n}$ in the following equivalent block-matrix notation:

$$\mathcal{A} = \left[\begin{array}{c|c} \mathbf{0} & \mathbf{I} \\ \hline A_1 & A_{2:s} \end{array}\right], \tag{19}$$

where $\mathbf{0} \in \mathbf{R}^{(s-1)n \times n}$ is a zero matrix, $\mathbf{I} \in \mathbf{R}^{(s-1)n \times (s-1)n}$ is an identity matrix, $A_1 \in \mathbf{R}^{n \times n}$ and $A_{2:s} \in \mathbf{R}^{n \times (s-1)n}$ is the following block matrix $A_{2:s} = [A_2 | \ldots | A_s]$.

For convenience, let us represent the augmented matrices X_{aug} and Y_{aug} defined in (13) as follows:

$$X_{aug} = \left[\begin{array}{c} X_1 \\ \hline X_2 \\ \hline \vdots \\ \hline X_s \end{array}\right] \quad \text{and} \quad Y_{aug} = \left[\begin{array}{c} X_2 \\ \hline X_3 \\ \hline \vdots \\ \hline X_{s+1} \end{array}\right], \tag{20}$$

where $X_i \in \mathbf{R}^{n\times(m-s)}$ denotes the sub-matrix

$$X_i = [\mathbf{z}_i|\mathbf{z}_{i+1}\ldots|\mathbf{z}_{m-s+i-1}] \tag{21}$$

for $i = 1, \ldots, s+1$.

Therefore the following equivalent presentations are valid:

$$X_{aug} = \left[\begin{array}{c} X_1 \\ \hline X_{2;s} \end{array}\right] \quad \text{and} \quad Y_{aug} = \left[\begin{array}{c} X_{2;s} \\ \hline X_{s+1} \end{array}\right], \tag{22}$$

where double indexing is used for block sub-matrix $X_{p;q}$:

$$X_{p;q} = \left[\begin{array}{c} X_p \\ \hline \vdots \\ \hline X_q \end{array}\right].$$

Then the relation (12) has the following equivalent representation:

$$\mathcal{A}X_{aug} = Y_{aug} \Leftrightarrow \left[\begin{array}{c|c} \mathbf{0} & \mathbf{I} \\ \hline A_1 & A_{2:s} \end{array}\right] \left[\begin{array}{c} X_1 \\ \hline X_{2;s} \end{array}\right] = \left[\begin{array}{c} X_{2;s} \\ \hline X_{s+1} \end{array}\right]. \tag{23}$$

Obviously, operator $\mathcal{A}$ can be represented as

$$\mathcal{A} = Y_{aug}X_{aug}^{\dagger}, \tag{24}$$

where $X_{aug}^{\dagger}$ is the Moore-Penrose pseudoinverse of X_{aug}. Eq. (24) implies

$$\mathcal{A} = \left[\begin{array}{c|c} \mathbf{0} & \mathbf{I} \\ \hline A_1 & A_{2:s} \end{array}\right] = \left[\begin{array}{c} X_{2;s} \\ \hline X_{s+1} \end{array}\right] X_{aug}^{\dagger}. \tag{25}$$

In order to calculate the block matrix $\mathcal{A}$ it is enough to calculate the last row of matrices:

$$A_{1:s} = [A_1|A_2|\ldots|A_s] = X_{s+1}X_{aug}^{\dagger}, \tag{26}$$

which is $n \times s.n$ matrix.

Reduced order DMD operator

Let us have a reduced SVD of $X_{aug} \in \mathbf{R}^{s.n\times(m-s)}$:

$$X_{aug} = U_X \Sigma_X V_X^*, \tag{27}$$

where $U_X \in \mathbf{R}^{s.n\times r}, V_X \in \mathbf{R}^{m-s\times r}, \Sigma_X \in \mathbf{R}^{r\times r}$, and let represent matrix U_X in a block matrix of the form (20)

$$U_X = \left[\begin{array}{c} U_1 \\ \hline U_2 \\ \hline \vdots \\ \hline U_s \end{array}\right], \tag{28}$$

with sub-matrices $U_i \in \mathbf{R}^{n\times r}$ for $i = 1, \ldots, s$.

Therefore, the reduced order DMD operator

$$\tilde{\mathcal{A}} = U_X^* \mathcal{A} U_X \tag{29}$$

has the following equivalent expression:

$$\tilde{\mathcal{A}} = [U_{1;s-1}^* \mid U_s^*] \left[\begin{array}{c|c} \mathbf{0} & \mathbf{I} \\ \hline A_1 & A_{2:s} \end{array}\right] \left[\begin{array}{c} U_1 \\ \hline U_{2;s} \end{array}\right], \tag{30}$$

where $\mathbf{0} \in \mathbf{R}^{(s-1)n\times n}$ is a zero matrix, $\mathbf{I} \in \mathbf{R}^{(s-1)n\times(s-1)n}$ is an identity matrix. Double indexing is used for block sub-matrices $U_{p;q}$ of the form:

$$U_{p;q} = \left[\begin{array}{c} U_p \\ \hline \vdots \\ \hline U_q \end{array}\right].$$

From (30), after simple transformations and using (26), we obtain the following representation:

$$\tilde{\mathcal{A}} = U_{1;s-1}^* U_{2;s} + \; U_s^* X_{s+1} V_x \Sigma_X^{-1}, \tag{31}$$

which is an $r \times r$ matrix. Therefore, matrix $\tilde{\mathcal{A}}$ in (31) is the reduced order approximation of $\mathcal{A}$, which corresponds to formula (17) in the standard HODMD approach.

Alternative Higher Order DMD algorithm

Now, we can formulate an alternative version of the HODMD approach considered in section 1.3:

Algorithm 1:	Alternative	Higher Order DMD
Input:	Snapshot data matrix $\mathcal{D}$, and rank reduction parameter r.	delay embedding parameter s
Output:	DMD eigenvalues Λ	and modes Φ
1: **Procedure** AHODMD($\mathcal{D}$, s, r)		
2:	X_{aug} and X_{s+1}	*(Define matrices as in (21))*
3:	$[U_X, \Sigma_X, V_X] = SVD(X_{aug}, r)$	*(Truncated r-rank SVD of X_{aug})*
4:	$U_1, U_{2;s}, U_{1;s-1}, U_s$	*(Define matrices as in (28))*
5:	$\tilde{\mathcal{A}} = U_{1;s-1}^* U_{2;s} + U_s^* X_{s+1} V_X \Sigma_X^{-1}$	*(Low rank approximation of $\mathcal{A}$)*
6:	$[W, \Lambda] = EIG(\tilde{\mathcal{A}})$	*(Eigen-decomposition of $\tilde{\mathcal{A}}$)*
7:	$\Lambda = \mathrm{diag}\{\lambda_i\}$	*(DMD eigenvalues of $\mathcal{A}$)*
8:	$\Phi = U_X W$	*(DMD modes of $\mathcal{A}$)*
9: **End Procedure**		

It can be easily verified that in particular, for $s = 1$, the proposed algorithm reduces to the standard DMD algorithm. In the rest of this study, we will show that Algorithm 1 gives results identical to the standard HODMD algorithm and at the same time is computationally more economical.

Although Algorithm 1 accepts as input the entire data matrix $\mathcal{D}$, the proposed scheme is also applicable to a pre-reduced data system $\hat{\mathcal{D}}$, as in the standard HODMD approach. In other words, one can first apply SVD to the entire snapshot matrix, including the spatial truncation, which defines at the beginning the spatial modes, the spatial complexity, and the reduced snapshots. Since in this way, implementing the new algorithm with large s is computationally cheap, a good strategy is to apply the algorithm to several sample values of s and compare the results to guess the appropriate value of s. The new algorithm turns out to be quite robust in connection with varying s.

Computational Cost and Memory Requirement

The main difference between the two considered approaches, standard and alternative HODMD, lies in the representation of the reduced DMD operator.

	Standard HODMD	*Alternative HODMD*
$\tilde{\mathcal{A}}$	$U_X^* Y_{aug} V_X \Sigma_X^{-1}$	$U_{1;s-1}^* U_{2;s} + \ U_s^* X_{s+1} V_X \Sigma_X^{-1}$
CC	$rsn(m-s) + r^2(m-s+1)$	$rn[r(s-1)+m-s] + r^2(m-s+1)$

Table 1: *Reduced DMD operators and computational costs (CC) for Standard HODMD and Alternative HODMD algorithms.*

We note that the standard HODMD method requires the three matrices U_X, Σ_X and V_X (from the SVD of X_{aug}) and the entire matrix Y_{aug}, the alternative HODMD method uses the first three matrices plus the matrix X_{s+1} instead of Y_{aug}. This suggests that the alternative approach would require less storage and computational work, given that $Y_{aug} \in \mathbf{R}^{s.n \times (m-s)}$ and $X_{s+1} \in \mathbf{R}^{n \times (m-s)}$. Table 1 gives a brief summary of the reduced DMD operators and the computational costs for the two approaches considered.

As we can see from Table 1, both DMD operators require matrix multiplication $V_X \Sigma_X^{-1}$ with the computational costs $r^2(m-s+1)$, so in the comparison we will reduce this operation for both cases.

Let us define the following two (reduced) cost functions:

$$\begin{aligned} f_1(s,r) &= rns(m-s), && (\textit{Alternative HODMD}) \\ f_2(s,r) &= rn\left[r(s-1)+m-s\right], && (\textit{Standard HODMD}). \end{aligned} \tag{32}$$

A three-dimensional visualization of the f_1 and f_2 functions is shown in Fig. 1 (for example values $n = 20$ and $m = 200$).

From (32), we see that for $s = 1$ (where s is the time-shift coefficient) they have the same computational complexity (because the two algorithms reduce to the standard DMD algorithm).

It can easily be deduced that the difference between the computational work of the standard approach and the alternative approach is equal to:

$$f_{diff} = f_2 - f_1 = rn(s-1)(m-r-s). \tag{33}$$

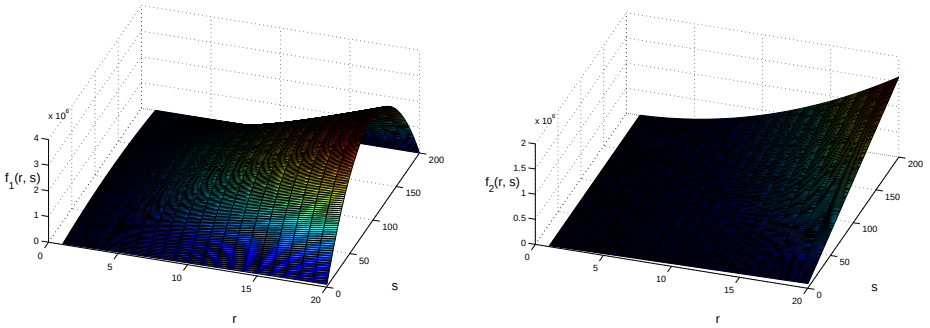

Figure 1: Computational cost functions: (*Left*) f_1 (standard HODMD) and (*Right*) f_2 (alternative HODMD), with $n = 20$ and $m = 200$.

If we consider f_{diff} in (33) as a function of a variable s (for a fixed value of r), then it has the following equivalent representation:

$$f_{diff} = -a_1 s^2 + a_2 s - a_3, \tag{34}$$

where $a_1 = rn$, $a_2 = rn(m-r+1)$ and $a_3 = rn(m-r)$. It can be shown that the two zeros of f_{diff} are 1 and $m-r$. Therefore, for the values of the time-shift coefficient s in the interval $[2, m-r]$, the *Alternative HODMD* is more efficient than the *Standard HODMD*. From the fact that it has the shape

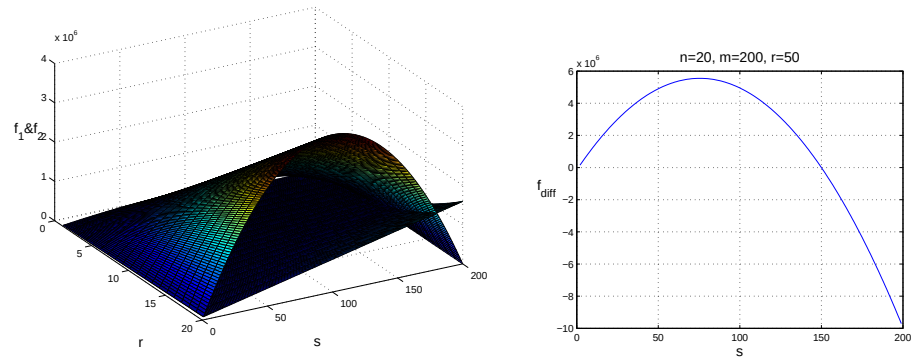

Figure 2: (*Left*) overlapped cost functions f_1 and f_2; (*Right*) function f_{diff}.

of a parabola, we can conclude that it reaches its maximum at the value $s = (m-r+1)/2$. Therefore, the *Standard HODMD* algorithm requires at

least the following number of operations:

$$f_{diff}(2) = rn(m - r - 2), \tag{35}$$

in more than the alternative algorithm, and this number can reach up to

$$\max_s f_{diff} = f_{diff}\left(\frac{m-r+1}{2}\right) = \frac{rn}{2}\left[(m-r+1)^2 - 2(m-r)\right]. \tag{36}$$

This can also be seen in the overlapping charts in Fig. 2 (*Left*).

Furthermore, in the standard approach the number of floating numbers that must be stored (to compute the reduced DMD operator) exceeds those in the alternative algorithm by: $n(s-1)(m-s)$.

So for example with a dataset consisting of 200 snapshots ($m = 200$) and each snapshot is of dimension 20 ($n = 200$), then the standard algorithm will calculate between $3.9e10^2 \times r$ and $2e10^5 \times r$ more operations, depending on the choice of the delay factor s, where r is the rank truncation index. The graph of f_{diff} is depicted in Fig. 2 (*Right*), for example values $n = 20$, $m = 200$ and $r = 50$).

3 Numerical examples

To demonstrate and compare the standard and alternative HODMD algorithms, we consider two illustrative examples.

Example 1: A toy model for the temporal evolution of LiDAR

In this example, we will demonstrate a fully data-driven application of the Alternative HODMD approach to feature extraction.

The model is defined as

$$z(x,t) = (2.10^{-3}x^3 + 8.10^{-2}x^2 + x)[2\sin(\omega_1 t) + 0.25\cos(\omega_2 t)],$$

where $\omega_1 = 2\pi/45$ and $\omega_2 = \sqrt{5}$. This example is taken from the book by Clainche and Vega [20], Chapter 7. It is representative of the methodology used in the prediction of the *Light Detection And Ranging* (LiDAR) measurements, see [21]. The exception is that this toy model is free of noise.

The dynamics associated with this model is multi-scale, since the two frequencies imposed exhibit quite different values (small and large), quasi-periodic, because ω_1 and ω_2 are incommensurable (namely, the ratio ω_1/ω_2 is not a rational number) and, consequently, fairly demanding. It is possible to represent this model as a DMD expansion involving four frequencies, namely

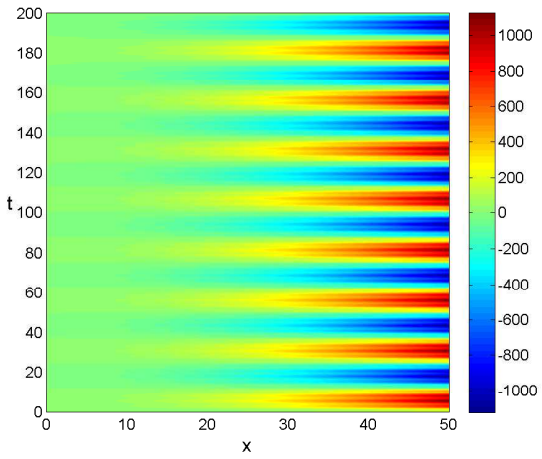

Figure 3: The model (1) defined in the interval $x \in [0, 50]$.

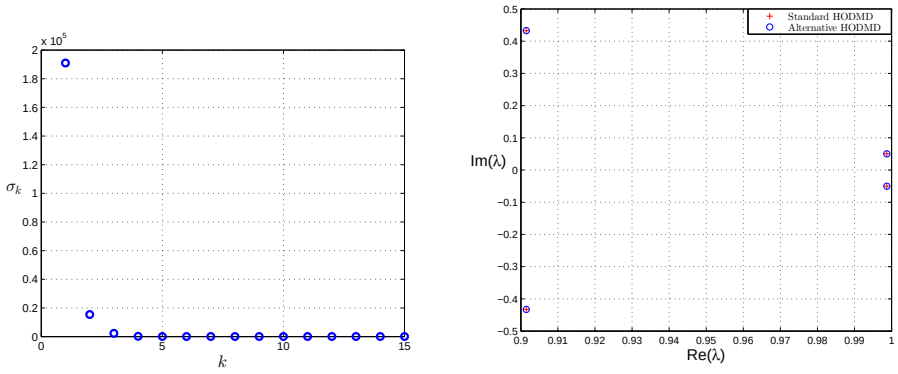

Figure 4: (*Left*) The first 15 singular values of X_{aug}, with $s = 4$ and $r = 4$; (*Right*) DMD eigenvalues computed by Standard HODMD (blue circles) and Alternative HODMD (red crosses).

$\pm\omega_1$ and $\pm\omega_2$. The spatio-temporal color map of the model is presented in Fig. 3. The model is spatially defined in the interval $x \in [0, 50]$.

A set of 1000 snapshots is collected in the time interval $t \in [0, 200]$. Using the standard DMD algorithm provides completely spurious results since the spatial complexity of this problem (represented by the number of singular values, n = 1) is smaller than the spectral complexity (represented by the number of frequencies defined in this model, r = 4). Thus s should be at

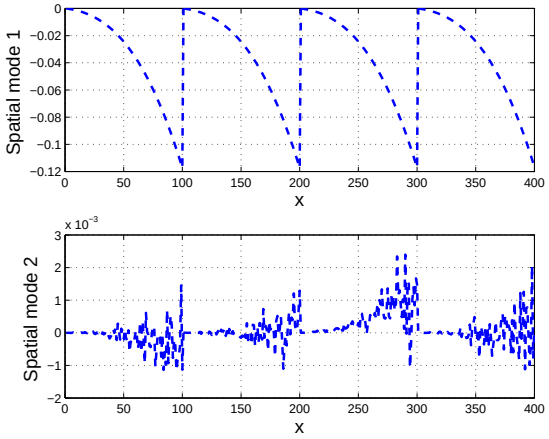

Figure 5: Two leading DMD modes of Standard HODMD method.

least 4, although in the examples presented the optimal solution is found for values of $s > 10$.

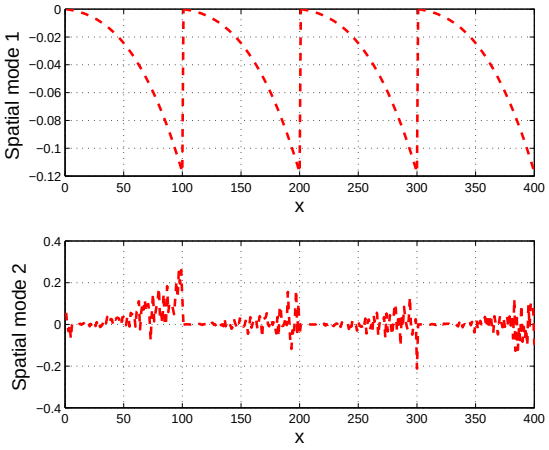

Figure 6: Two leading DMD modes of Alternative HODMD method.

By setting s in the interval $s \in [10, 100]$, the relative RMS error in the reconstruction of the original snapshots using both HODMD algorithms is $\sim 10^{-14}$. Fig. 4 shows the singular values calculated in the dimension-reduction step of the HODMD algorithm.

When using the values $s = 4$ and $r = 4$, both algorithms achieve the same accuracy with an error of $1.4e-11$ and $4.7e-11$, respectively. Increasing the values of $s = 4$ and/or $r = 4$, the accuracy of both algorithms increases. The two algorithms produce identical DMD eigenvalues, see Fig. 4 and comparable DMD modes, see Fig. 5 and Fig. 6. As expected, the method identifies four exact frequencies, namely $\pm\omega_1$ and $\pm\omega_2$, and reconstructs the original data with a RMS error $\sim 10^{-14}$.

Example 2: Van der Pol oscillator

Now, we consider the classical Van der Pol oscillator model. It is described by B. van der Pol in [22], defined as

$$\ddot{x} - \mu(1 - x^2)\dot{x} + x = 0,$$

where the usual meaning of $x(t)$ is position, but this may differ depending on the application, and μ is a scalar parameter that characterizes damping. If the time derivative $y(t) = \dot{x}(t)$ is introduced as an additional variable, the

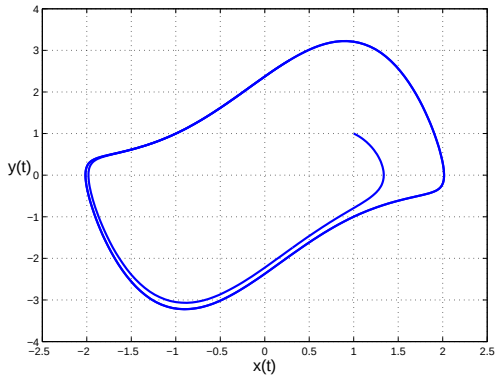

Figure 7: Trajectory of the Van der Pol oscillator.

equation can be reduced to a system of first order differential equations

$$\begin{aligned} \dot{x} &= y \\ \dot{y} &= \mu(1 - x^2)y - x\,. \end{aligned} \tag{37}$$

The parameter $\mu > 0$ controls the degree of nonlinearity; we use the value $\mu = 1.5$. Time-domain simulations are performed by using discretization time-steps of $\triangle t = 0.02$ over a total time period of $T = 20$.

The differential equation is solved in MATLAB with ode45 solver. The generated data matrix $\mathcal{D}$ is of dimension 2×1000. Simulation results from initial conditions $[x_0, y_0] = [1, 1]$ are shown in Fig. 7. Standard DMD ap-

$s=$	$r=$	*Standard HODMD*	*Alternative HODMD*
50	12	$4.822e-01$	$4.823e-01$
80	15	$4.621e-01$	$4.593e-01$
100	20	$3.622e-01$	$3.583e-01$
200	40	$5.30e-02$	$5.23e-02$
250	50	$2.59e-02$	$2.57e-02$
300	70	$1.5e-03$	$1.5e-03$
350	80	$1.3745e-04$	$1.3912e-04$

Table 2: *RMS error of reconstruction by Standard HODMD and Alternative HODMD.*

proach provides spurious results in reconstruction of the dynamics (37), because it identifies only two modes that are insufficient to approximate the dynamics. In order to achieve a better approximation, we used different values for s and r. Table 2 shows the RMS error for different values of s and r for the two algorithms. As we can see from Table 2 by increasing the

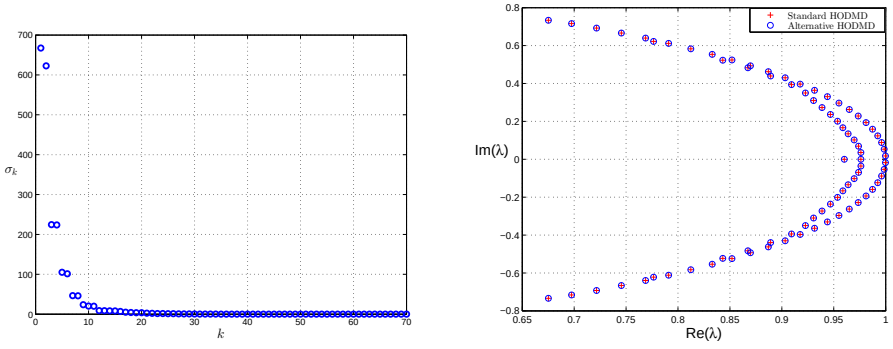

Figure 8: Left: The first 70 singular values of X_{aug}; Right: DMD eigenvalues computed by Alternative HODMD method, with $s = 300$ and $r = 70$.

values of s and/or r the accuracy of both algorithms increases also. For the

value $s = 300$ the first 70 singular values of the augmented data matrix X_{aug} are shown in Fig. 8 (left). In this case, according to formula (33), we can calculate that the standard HODMD algorithm uses 2.6×10^7 calculations more than the alternative HODMD algorithm. By choosing $r = 70$, both algorithms achieve accuracy with an error of: $1.5e-3$. The DMD eigenvalues, calculated by both algorithms, are shown in Fig. 8 (right).

Two trajectories for $x(t)$ and $y(t)$ reconstructions of (37) using Standard HODMD and Alternative HODMD are shown in Fig. 9.

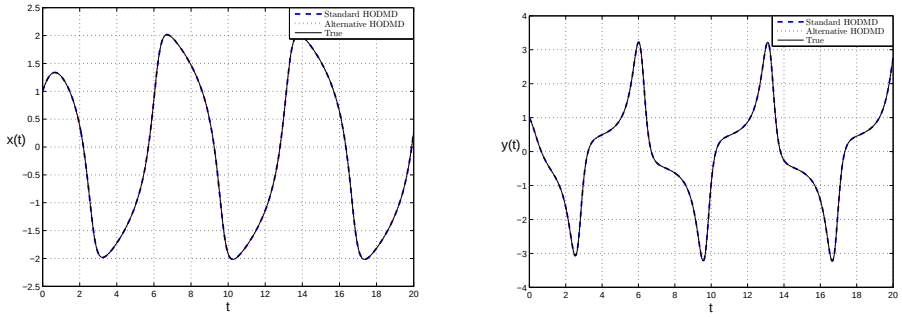

Figure 9: Reconstruction of $x(t)$ and $y(t)$ using Standard HODMD and Alternative HODMD methods.

The phase portrait reconstructions for the Van der Pol oscillator, by the two, Standard HODMD and Alternative HODMD, approaches are shown in Fig. 10.

4 Conclusion

We have provided a new algorithm for computing higher order dynamic mode decomposition from time series data. We show via simulation examples that the proposed algorithm can provide an identical approximation of the dynamics regarding more cost effectiveness than the standard HODMD approach. The new method has been illustrated and tested in several models: a spatio-temporal toy model, with application in the analysis of LiDAR experimental data, and the canonical Van der Pol oscillator model. Experimental results show that the introduced approach gives identical results to those of the standard HODMD method. In this way the introduced algorithm is an alternative to the standard HODMD algorithm and can be used in various fields of application.

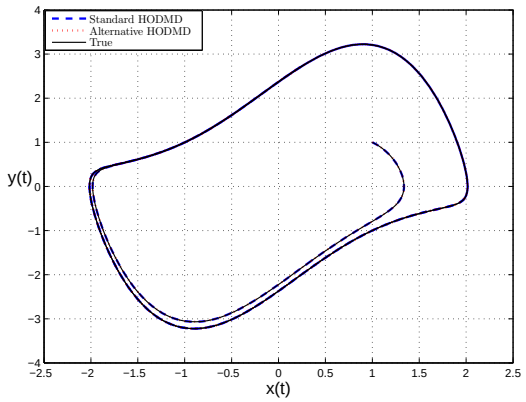

Figure 10: Reconstruction of the Van der Pol oscillator using Standard HODMD and Alternative HODMD methods.

References

[1] P.J. Schmid and J. Sesterhenn, Dynamic mode decomposition of numerical and experimental data. In *61st Annual Meeting of the APS Division of Fluid Dynamics*, American Physical Society, 2008.

[2] C.W. Rowley, I. Mezić, S. Bagheri, P. Schlatter, and D.S. Henningson, Spectral analysis of nonlinear flows, *J. Fluid Mech.* 641 (2009), 115-127.

[3] I. Mezić, Spectral properties of dynamical systems, model reduction and decompositions, *Nonlinear Dynam.* 41(1-3) (2005), 309-325.

[4] K.K. Chen, J.H. Tu, and C.W. Rowley, Variants of dynamic mode decomposition: Boundary condition, Koopman, and Fourier analyses, *J. Nonlinear Sci.* 22 (2012), 887-915.

[5] M.R. Jovanović , P. Schmid, J.W. Nichols, Sparsity-promoting dynamic mode decomposition, *Physics of Fluids* 26(2) (2014), 024103.

[6] B.R. Noack, W. Stankiewicz, M. Morzyski, P. Schmid, Recursive dynamic mode decomposition of transient and post-transient wake flows, *J. Fluid Mech.* 809 (2016), 843-72.

[7] C.W. Rowley, S.T. Dawson, Model reduction for flow analysis and control, *Annu. Rev. Fluid Mech.* 49 (2017), 387-417.

[8] P.J. Schmid, Dynamic mode decomposition and its variants, *Annu. Rev. Fluid Mech.* 54 (2022), 225-254.

[9] P.J. Schmid, Dynamic mode decomposition of numerical and experimental data, *J. Fluid Mech.* 656 (2010), 5-28.

[10] I. Mezić, Analysis of fluid flows via spectral properties of the Koopman operator, *Annu. Rev. Fluid Mech.* 45 (2013), 357-378.

[11] S. Bagheri, Koopman-mode decomposition of the cylinder wake, *J. Fluid Mech.* 726 (2013), 596-623.

[12] J.H. Tu, C.W. Rowley, D.M. Luchtenburg, S.L. Brunton, J.N. Kutz, On dynamic mode decomposition: Theory and applications, *J. Comput. Dyn.* 1(2) (2014), 391-421.

[13] J.N. Kutz, S.L. Brunton, B.W. Brunton, and J. Proctor, *Dynamic Mode Decomposition: Data-Driven Modeling of Complex Systems*, SIAM, ISBN 978-1-611-97449-2, 2016.

[14] Z. Bai, E. Kaiser, J.L. Proctor, J.N. Kutz, S.L. Brunton, Dynamic Mode Decomposition for CompressiveSystem Identification, *AIAA Journal*, 58(2) (2020), 561-574.

[15] S. Le Clainche and J.M. Vega, Higher order dynamic mode decomposition, *SIAM J. Appl. Dyn. Syst.* 16(2) (2017), 882-925.

[16] H. Arbabi and I. Mezić, Ergodic Theory, Dynamic Mode Decomposition, and Computation of Spectral Properties of the Koopman Operator, *SIAM J. Appl. Dyn. Syst.* 16 (2017), 2096-2126.

[17] S.L. Brunton, B.W. Brunton, J.L. Proctor, E. Kaiser, and J.N. Kutz, Chaos as an intermittently forced linear system, *Nat. Commun.*, 8 (2017), 1-9.

[18] M. Kamb, E. Kaiser, S.L. Brunton and J.N. Kutz, Time-delay observables for Koopman: Theory and applications, *SIAM J. Appl. Dyn. Syst.* 19 (2020), 886-917.

[19] F. Takens, *Detecting strange attractors in turbulence, in Dynamical Systems and Turbulence*, Lecture Notes in Math. 898, Springer, Berlin, 1981.

[20] S. Le Clainche and J.M. Vega, *Higher Order Dynamic Mode Decomposition and Its Applications*, Academic Press, Elsevier, ISBN 978-0-12-819743-1, 2020.

[21] S. Le Clainche, L.S. Lorente, J.M. Vega, Wind Predictions Upstream Wind Turbines from a LiDAR Database, *Energies* 11(3) (2018), 543.

[22] B. Van der Pol, LXXXVIII. On relaxation-oscillations, *Phil. Mag.* 2(11) (1926), 978-992.